Journal of Power Sources 240 (2013) 149–154

Contents lists available at SciVerse ScienceDirect

Journal of Power Sources

journal homepage: www.elsevier.com/locate/jpowsour

Short communication

SnO_2/graphene composite as highly reversible anode materials for lithium ion batteries

Qi Guo, Zhe Zheng, Hailing Gao, Jia Ma, Xue Qin*

School of Science, Tianjin University, No. 92 Weijin Road, Tianjin 300072, China

HIGHLIGHTS

- We explored a facile method for the preparation of SnO_2/graphene composite.
- The SnO_2 nanoparticles are uniformly coated on the graphene nanosheets.
- The graphene is of high degree of purity.
- The initial discharge capacity is as high as 1995.8 mAh g^{-1} at the current density of 1 A g^{-1}.
- After 40 cycles the reversible discharge capacity is still remained at 1545.7 mAh g^{-1}.

ARTICLE INFO

Article history:
Received 15 January 2013
Received in revised form
19 March 2013
Accepted 25 March 2013
Available online 1 April 2013

Keywords:
Tin oxide
Graphene
Composite
Lithium-ion batteries

ABSTRACT

Tin oxide (SnO_2)/graphene composite is synthesized via a simple wet chemical method using graphene oxide and $SnCl_2 \cdot 2H_2O$ as raw materials. Graphene of high reduction degree in the composite can provide high conductivity and large-current discharge capacity. SnO_2 nanoparticles with dimension around 5 nm are uniformly distributed on the graphene matrix.

The SnO_2/graphene composite exhibits outstanding electrochemical performance such as high reversible capacities, good cycling stability and excellent high-rate discharge performance. The initial discharge and charge capacities are 1995.8 mAh g^{-1} and 1923.5 mAh g^{-1}, respectively. After 40 cycles, the reversible discharge capacity is still maintained at 1545.7 mAh g^{-1} at the current density of 1 A g^{-1}, indicating that the composite is a promising alternative anode material used for high-storage lithium ion batteries.

1. Introduction

Lithium-ion batteries are regarded as the promising power source for portable electrical devices and electrical/hybrid vehicles due to their high electromotive force and high energy density [1,2]. Graphite, as anode material, has been widely used owing to its extraordinary electronic transport properties, large surface area, and high electrocatalytic activities although its limited specific capacity (372 mAh g^{-1}) cannot fulfil the increasing demand for lithium-ion batteries with higher energy density [3–5]. To settle this problem, many studies have been taken into consideration to investigate new electrode materials and metal oxide/graphene composites are selected as a kind of promising material for lithium-ion batteries as their specific capacities are much higher than graphene [6,7].

Among them, SnO_2, an *n*-type and wide band gap semiconductor, has attracted much attention as an anode material for the new-generation lithium-ion batteries with its high theoretical capacity (790 mAh g^{-1}) [8,9]. However, it suffers from large volume changes and agglomeration associated with the Li-ion insertion and extraction processes, which brings about failure and loss of electrical contact of the anode [10,11]. In addition, there is also a huge irreversible capacity during the first cycle due to the formation of amorphous Li_2O matrix.

In order to address the problems discussed above, SnO_2/graphene composite which can take both advantages of SnO_2 and graphene has been prepared and its synthesis has drawn tremendous research interest for further application in the anode of lithium-ion batteries [12–14].

Here, we develop a simple wet chemical method to obtain SnO_2/graphene composite. The as-prepared composite can possess both of the advantages of tin oxide and graphene and exhibits superior electrochemical performance with large reversible capacity, excellent cycling performance and good rate capability. Compared

* Corresponding author. Tel.: +86 022 27403670.
E-mail address: qinxue@tju.edu.cn (X. Qin).

0378-7753/$ – see front matter
http://dx.doi.org/10.1016/j.jpowsour.2013.03.116

to other similar composites, this SnO_2/graphene composite could be obtained via an easier method but exhibits much higher specific capacities at large current density.

2. Experimental

2.1. Sample preparation

The SnO_2/graphene composite was synthesized using a wet chemical method. All chemicals were of analytical grade. The graphene oxide employed here was synthesized from natural graphite by a modified Hummers' method [15,16].

Dried graphene oxide of 0.1 g was added into 100 mL distilled water. The obtained mixture was ultrasonicated for 15 min in the ultrasonic cell crusher. Then the suspension was centrifuged for 20 min at 4000 r min^{-1} and the supernatant was used for the next step reaction, the resultant graphene oxide solution was labelled as solution A. Solution B was prepared by dissolving 0.1 g of tin chloride dehydrate in 100 mL of distilled water with some appropriate concentrated hydrochloric acid. The two solutions were mixed and transferred to a 250 mL three distillation flask in which the above mixture was refluxed at 80 °C in an oil bath for 12 h under stirring. After standing for another 24 h, the system was cooled down to room temperature. The as-prepared products were rinsed with distilled water until the pH value of the solution reached to neutral and then dried at 50 °C for 12 h. The bare SnO_2 nanoparticles were synthesized under the same condition except replacing the graphene oxide with hydrogen peroxide as oxidizing agent.

2.2. Sample characterization

The structure and morphology of the as-prepared SnO_2/graphene composite were characterized by X-ray diffraction (XRD, D/MAX-2500), Raman spectroscopy (In Via Reflex), Transmission electron microscopy (TEM, Tecnai G2 F20), X-ray photoelectron spectroscopy (XPS, PHI1600) and Thermogravimetric analysis (TGA, STA 409 PC Luxx®).

2.3. Electrochemical measurements

The working electrodes were prepared by mixing 80 wt% as-prepared active materials with 10 wt% acetylene black and 10 wt % polyvinylidene fluoride (PVdF) binder in *N*-methyl-2-pyrrolidinone (NMP) to form homogeneous slurry through grinding in a mortal. Then the slurry was pasted onto a copper foil substrate and dried in vacuum oven at 120 °C for at least 12 h. The electrochemical cells used this active materials as the working electrode, Li foil as counter electrode and reference electrode, and 1 mol L^{-1} $LiPF_6$ in a 1:1 (volume:volume) mixture of ethylene carbonate (EC) and dimethyl carbonate (DMC) as the electrolyte which was assembled in an argon-filled glove box. The calculation of the capacity of the composites was based on the SnO_2/graphene composites. The cells were galvanostatically charge–discharge in the voltage range 0.01–2.5 V vs. Li/Li^+ by a battery testing system (LAND CT-2001A system). Cyclic voltammetry (CV) curves were collected using Zahner Ennium electrochemical workstation. Electrochemical impedance spectra of the electrodes were recorded from 100 kHz to100 mHz at 5 mV of the amplitude of the perturbation.

3. Results and discussion

Fig. 1 shows the XRD patterns of graphene and the as-prepared SnO_2/graphene composites. The peaks at about $2\theta = 26°$ and

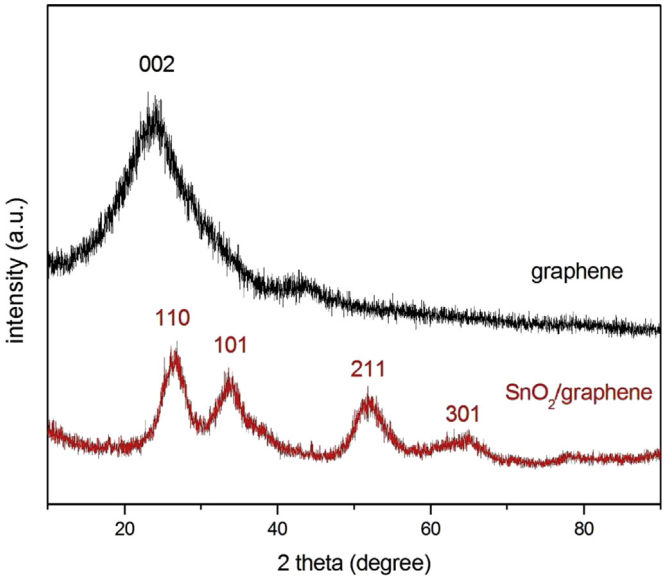

Fig. 1. XRD patterns of graphene and SnO_2/graphene composite.

$2\theta = 43°$ can be assigned to the [002] and [100] plane of graphene nanosheets [17]. The diffraction peaks for the crystalline SnO_2 nanoparticles are clearly observed. The four intense diffraction peaks at $2\theta = 26.06°$, 33.04°, 51.76°and 65.04°can be indexed as the (110), (101), (211), (301) plane of the standard tetragonal SnO_2 phase, respectively. The quite broadened diffraction peaks indicate the small sizes of the SnO_2 nanoparticles, which will contribute to the high electrochemical performance.

The as-product was also characterized by Raman spectroscopy. As shown in Fig. 2, a weak peak at about 621 cm^{-1} confirms the presence of SnO_2 [18,19]. The peaks at about 1342 cm^{-1}, 1592 cm^{-1} are assigned to the D and G band of graphene, respectively, and the intensity ratio of the D to G band (I_D/I_G) is as high as 1.8, revealing that most of the oxygen functional groups intercalated into the interlayer spacing of graphite have been removed during the GO reduction process. The peaks at about 2676 cm^{-1}, 2929 cm^{-1} are assigned to the 2D and D + G band of graphene [20], respectively, which also suggests the substantial removal of oxygen containing groups during the GO reduction process. Graphene of high

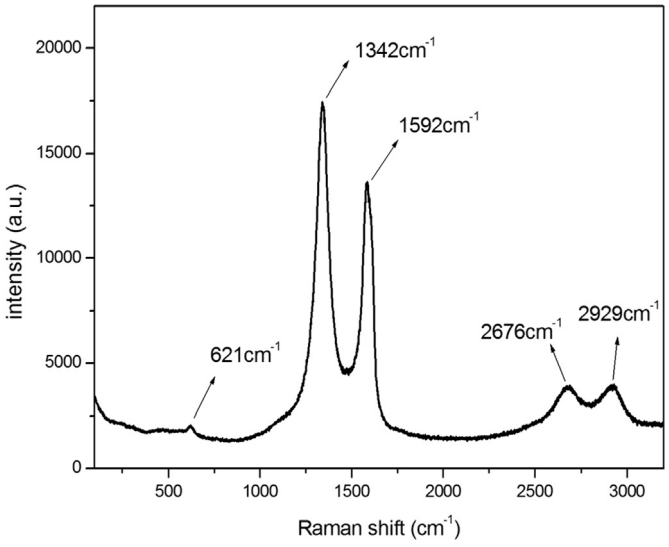

Fig. 2. Raman spectrum of SnO_2/graphene composite.

reduction degree can provide high conductivity and large-current discharge capacity.

The graphene nanosheets are partially overlapped as shown in the low-resolution TEM image of SnO_2/graphene composite (Fig. 3a). Fig. 3b is a TEM image of the raw material graphene oxide as a contrast to Fig. 3c where SnO_2 nanoparticles are uniformly coated on the surface of graphene. Fig. 3d is a high-resolution TEM image of SnO_2/graphene from which we can see layered structures of graphene decorated with homogeneously SnO_2 nanoparticles whose size is about 5 nm, and the small stripes of the prints indicate good crystal lattices of SnO_2.

XPS analysis was conducted in the range of 0–1100 eV to investigate the surface composition and chemical states in the SnO_2/graphene composites. Fig. 4a shows the wide-survey XPS spectrum of the SnO_2/graphene, which attributes to the existence of C, O, Sn. In addition, the intense peaks of Sn and O suggest the presence of a great amount of SnO_2 nanoparticles. As depicted in Fig. 4b, SnO_2/graphene shows three different C 1s building energies, 284.6 eV for non-oxygenated C, 286.3 eV for carbon in C–O and 288.5 eV for carbonyl carbon (C=O), respectively. The peak of C–O species is quite weak, which indicates the oxygen containing groups have been removed by the Sn^{2+} ions as well as certifies that the Sn^{2+} ions lead to the reduction process of GO. Moreover, the presence of SnO_2 can be proved by the Sn3d spectrum (Fig. 4c) in which two outstanding peaks are attributed to $Sn3d_{5/2}$ and $Sn3d_{3/2}$.

The thermal properties and the compositions of the as-prepared products were characterized by thermogravimetric analysis (TGA) in air. TGA curves of the SnO_2/graphene are shown in Fig. 5. An abrupt weight loss occurs from 350 °C to 650 °C, indicating the oxidization of graphene [21]. After 650 °C, there is no further mass loss. The stability of the trace indicates the complete removal of graphene. According to the TGA curves, 58 wt% of SnO_2 are coated on the surface of graphene nanosheets.

The electrochemical reactivity of the SnO_2/graphene composite as anode in lithium-ion batteries was evaluated by cyclic voltammetry (CV) in the potential range of 0.01 V–2.5 V with scanning rates of 0.2 mV s^{-1}, 0.5 mV s^{-1}, 1 mV s^{-1}, 2 mV s^{-1},respectively. As seen in Fig. 6, there is a small cathodic peak in each curve, which can be ascribed to the formation of the solid electrolyte (SEI) layers at the surface of active materials [22] as well as the reduction of SnO_2 to Sn with the synchronous formation of Li_2O and the Li insertion in graphene nanosheets to form Li_xC (Eqs. (1) and (3)). In the anodic curve, the oxidation peak around 0.5–0.85 V can be assigned to Li extraction from graphene nanosheets, which is most likely due to the Li de-alloying from Li_xSn (Eq. (2)). The other oxidation peak around 1.25–1.75 V can be attributed to a conversion reaction occurring between Li_2O and metallic Sn (Eq. (4)) [23] as well as partly reversible reaction of the Eq. (1) [24]. Even though the scanning rate changes, the positions of the oxidation peaks do not move much, which indicates the SnO_2/graphene composite has

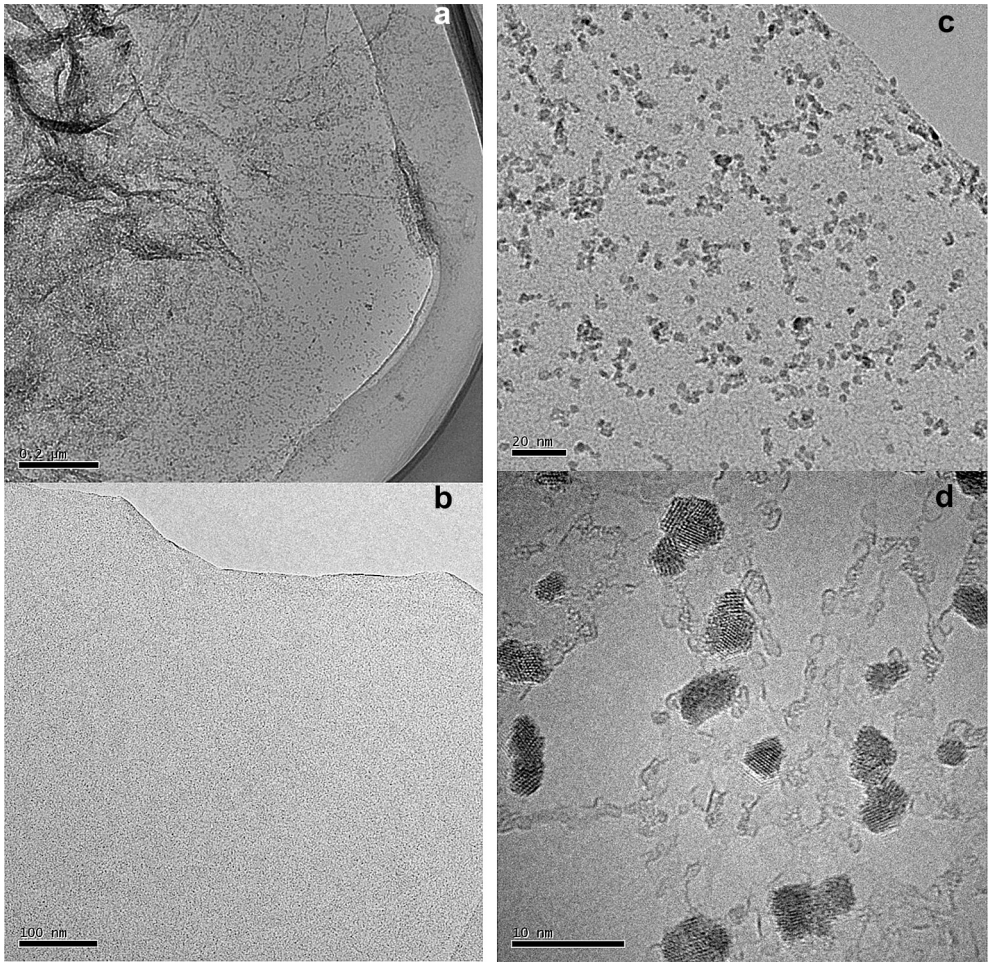

Fig. 3. Transmission electron microscopy images of the SnO_2/graphene composite (a, c, d) and graphene oxide (b).

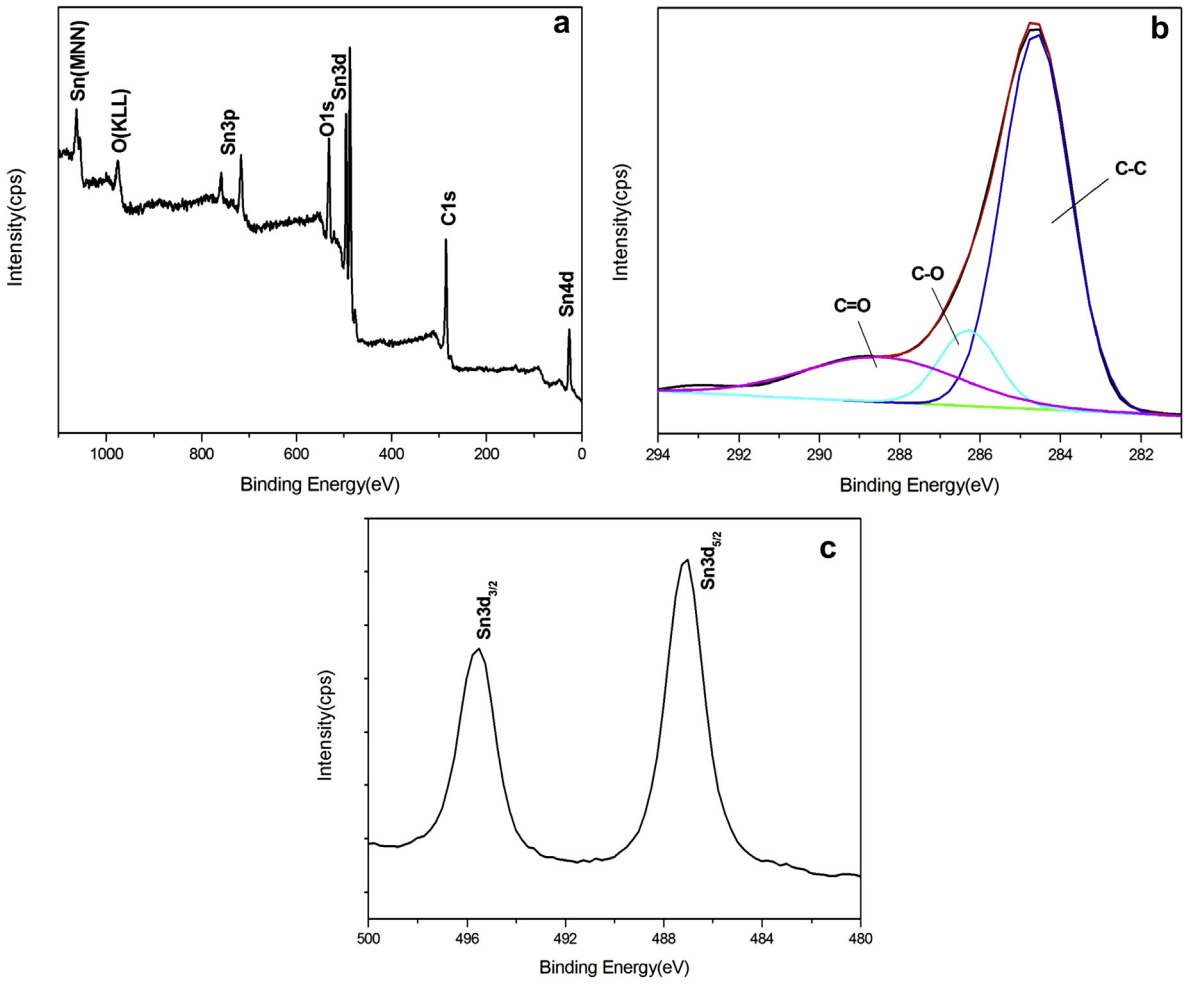

Fig. 4. XPS spectrum of the SnO_2/graphene (a), C1s (b), Sn3d (c).

an excellent cycling performance and good large-current discharge capacity due to the high conductivity of graphene.

$$4Li^+ + SnO_2 + 4e^- \rightarrow Sn + 2Li_2O \quad (1)$$

$$xLi^+ + Sn + xe^- \leftrightarrow Li_xSn \quad (2)$$

$$xLi^+ + C\ (graphene) + xe^- \leftrightarrow Li_xC \quad (3)$$

$$Li_2O + Sn \leftrightarrow SnO + 2Li^+ + 2e^- \quad (4)$$

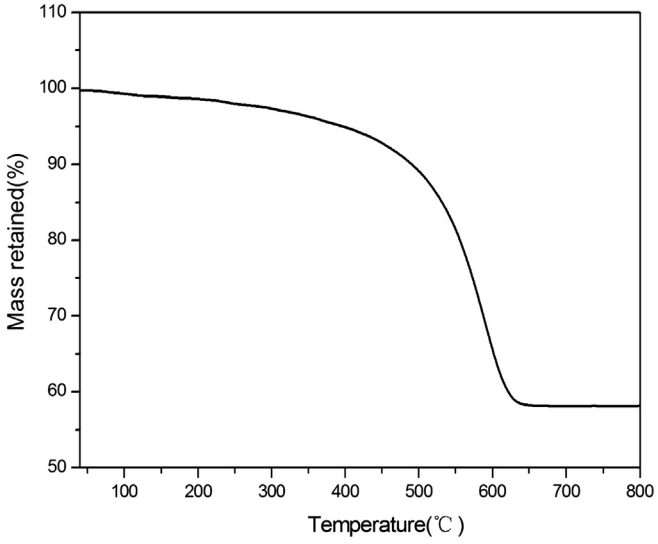

Fig. 5. TGA curve of the SnO_2/graphene in air.

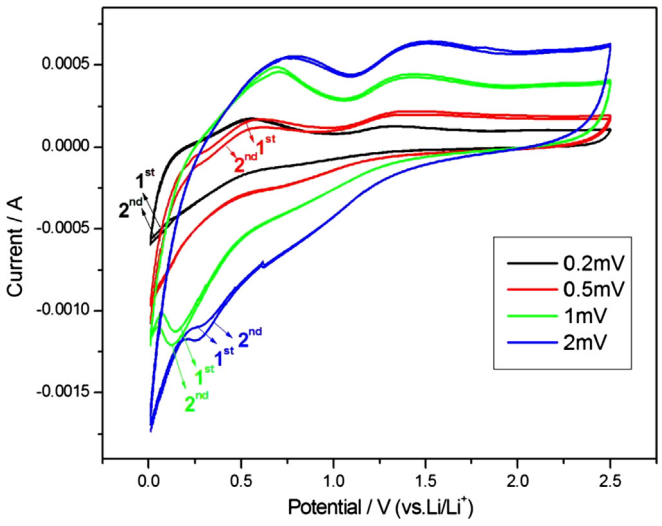

Fig. 6. CV curves of the SnO_2/graphene composite.

The electrochemical performance of the SnO_2/graphene composite was evaluated via galvanostatic charge/discharge cycling at the current density of 1 A g^{-1} with the voltage range from 0.01 to 2.5 V. For comparison, the SnO_2 nanoparticles were also tested. Fig. 7a and b show the typical charge/discharge profiles of SnO_2/graphene and SnO_2 nanoparticles in the first two cycles. The initial discharge specific capacity of the SnO_2/graphene composite is 1995.8 mAh g^{-1} with a reversible specific capacity of 1923.5 mAh g^{-1} while the SnO_2 nanoparticles are 859.1 mAh g^{-1} and 689 mAh g^{-1}, respectively. Obviously, the initial coulombic efficiency of the SnO_2/graphene composite is as high as 96.4%, which is higher than that of the bare SnO_2 nanoparticles (80.2%). The large-current discharge capacity of the composites mainly results from the formation of the Li_xSn alloy during the charging and discharging process [Eq. (2)] as well as the conversion reaction of Eq. (4). And it also can be attributed to the high reduction degree of graphene and the uniform distribution of SnO_2 nanoparticles on graphene nanosheets. This characteristic has never been explored and is highly desirable and important. The interaction between the two composites results to a much higher electrochemical capacitance than either of graphene or SnO_2, which suggest that the SnO_2 nanoparticles decorated graphene improves several properties of the composite such as the electronic and ionic conductivity, decreases of the polarization of the charge/discharge processes [23].

The electrochemical cycling performances of the SnO_2/graphene composite and bare SnO_2 nanoparticles were investigated at the current density of 1 A g^{-1} (Fig. 8). The SnO_2/graphene composite exhibits a high initial discharge specific capacity of 1995.8 mAh g^{-1} (Fig. 8a). The first charge capacity is 1923.5 mAh g^{-1} which could remain about 1707.7 mAh g^{-1} up to 10 cycles. And even after 40 cycles, the reversible discharge capacity is still remained at 1545.7 mAh g^{-1}. On the other hand, the SnO_2 nanoparticles present a poor cycling performance (Fig. 8b). The severe pulverization leads to a rapid fading of capacity and the charge capacity reduces rapidly from 689 mAh g^{-1} to 237.2 mAh g^{-1} after 40 cycles. Compared with the bare SnO_2 nanoparticles, the SnO_2/graphene composite shows superior charge capacity and cycling performance. This can be ascribed to the uniform distribution of SnO_2 nanoparticles on graphene, which fully utilizes SnO_2 to release the stress caused by the drastic volume variation during the lithium intercalation/deintercalation process. With the increasing of cycle numbers, the curves of discharge and charge are getting closer and closer, which proves the excellent cycling stability of the SnO_2/graphene composite.

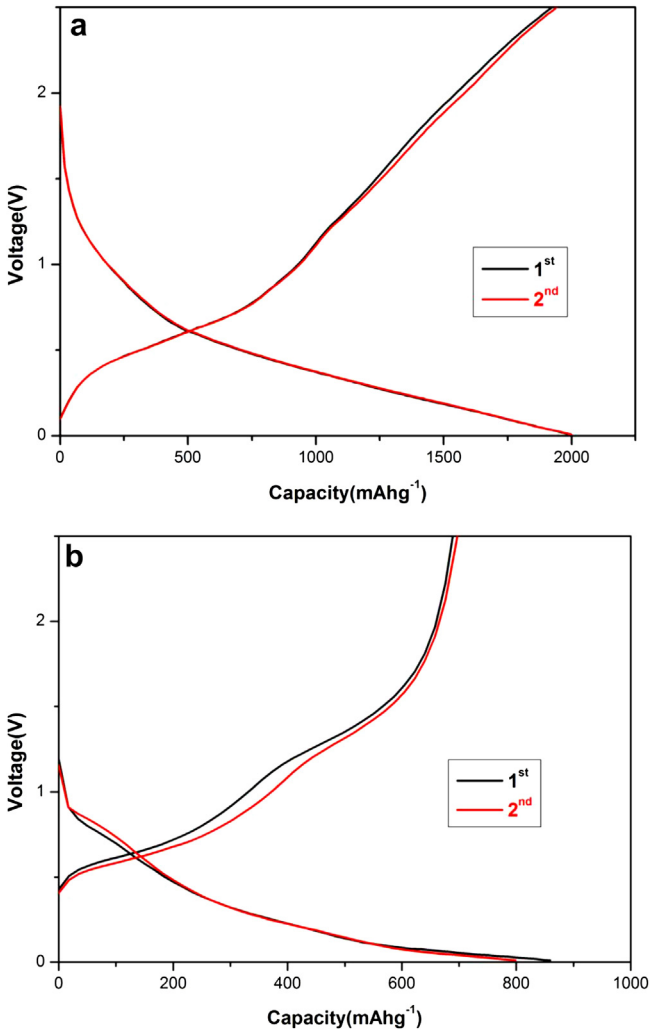

Fig. 7. Charge/discharge profiles of the SnO_2/graphene composite (a) and bare SnO_2 nanoparticles (b) for the 1st and 2nd.

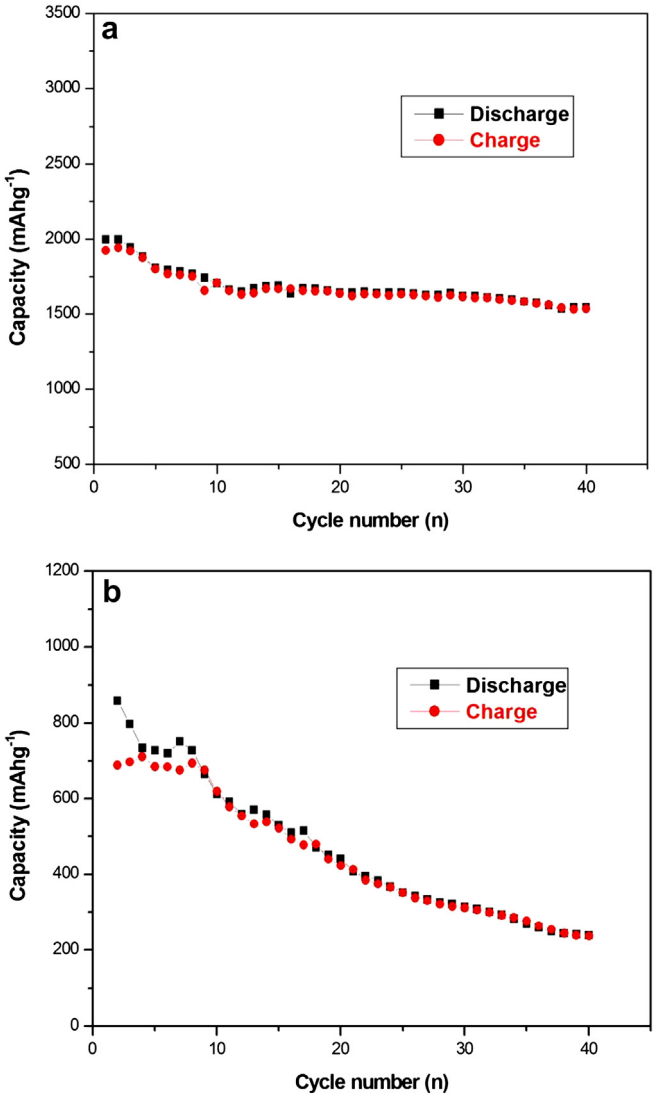

Fig. 8. Capacities vs. cycle number for SnO_2/graphene composite (a) and bare SnO_2 nanoparticles (b) at the current density of 1 A g^{-1}.

In order to verify the electrochemical performance of the composite in comparison with pure SnO_2 nanoparticles, electrochemical impedance spectroscopy measurements were carried out. Fig. 9 shows the electrochemical impedance spectra of SnO_2/graphene composite and the bare SnO_2 nanoparticles electrodes after 3 charge/discharge cycles as well as their simulated spectra respectively. As shown in Fig. 9, the Nyquist plots of both SnO_2/graphene composite and the SnO_2 nanoparticles consist of two semicircles and a slope. The equivalent circuit of the electrodes is shown in Fig. 10 where R1, R2, R3, W1 are denoted as solution resistance, SEI film resistance, reaction resistance and Warburg impedance, respectively. A constant phase element is expressed as CPEi (CPEi = $\{Yi(jw)\}^{-1}$). A nonlinear, least-square fitting calculation is performed using the equivalent circuit shown in Fig. 10. For SnO_2/graphene composite electrode, the electrochemical impedance value (R3) and CPE2 value (T) are 54.5 Ω cm^{-2} and 112 μF cm^2, and SnO_2 nanoparticles electrode are 101.4 Ω cm^{-2} and 74 μF cm^2. The value of CPE2 value (T) is suggested to be the value of the double layer capacitance of the electrode and related to the true reaction areas of the electrode. So the true reaction area of SnO_2/graphene composite electrode is larger than that of the SnO_2 electrode. The electrochemical impedance of the SnO_2/graphene composite electrode is lower than that of the SnO_2 nanoparticles electrodes, which leads to a higher electrochemical activity of the SnO_2/graphene composite electrode. This result shows that graphene in the composite can largely enhance the electrochemical activity of SnO_2 nanoparticles during the cycle processes.

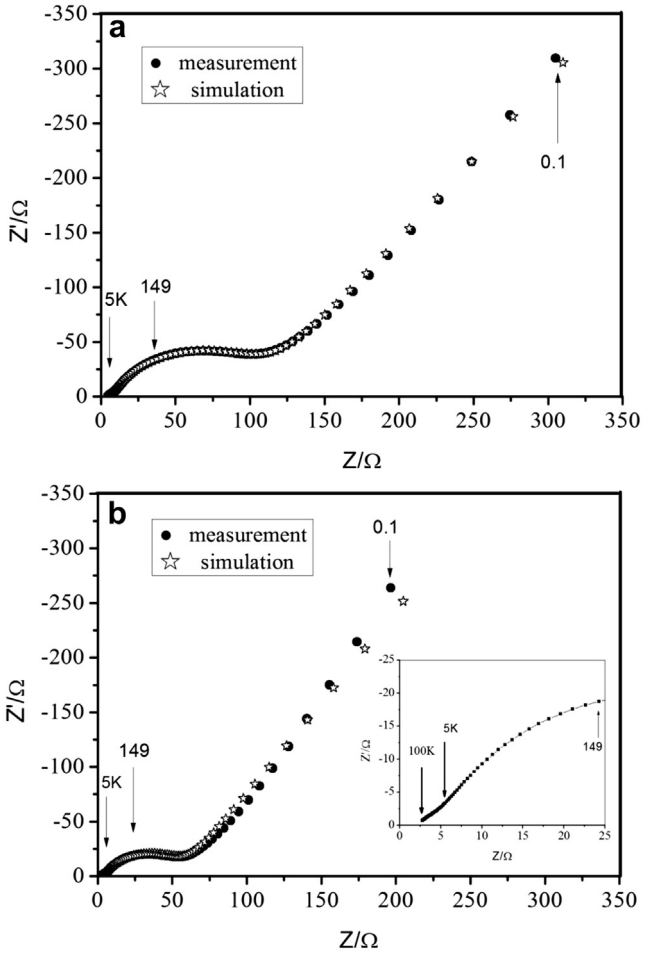

Fig. 9. Electrochemical impedance spectra of bare SnO_2 nanoparticles electrode (a) and SnO_2/graphene electrode (b).

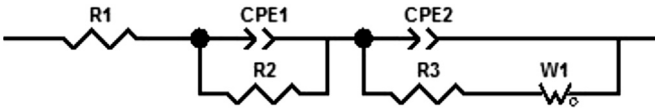

Fig. 10. The equivalent circuit of the bare SnO_2 electrode and SnO_2/graphene electrode.

4. Conclusions

SnO_2/graphene composite with uniform SnO_2 nanoparticles coating was prepared by a simple wet chemical method. The as-prepared products exhibited an excellent lithium intercalation/deintercalation performance as anode materials for lithium-ion batteries. Our composite displayed large specific capacities especially at high current density. All of the superior electrochemical properties were ascribed to the high purity of graphene, the homogeneously dispersion and thin-layered SnO_2 on graphene. Our results could facilitate the practical applications of SnO_2/graphene composite in lithium-ion battery anodes.

Acknowledgements

The authors gratefully acknowledge the financial support from the National Natural Science Foundation of China (20603024) and the Open Project of Key Lab Adv. Energy Mat. Chem. (Nankai Univ.) (KLAEMC-OP201201).

References

[1] Li-Li Xing, Chun-Hua Ma, Chun-Xiao Cui, Xin-Yu Xue, Solid State Sci. 14 (2012) 111–116.
[2] Konda Shiva, H.B. Rajendra, K.S. Subrahmanyam, Aninda J. Bhattacharyya, C.N.R. Rao, Chem. Eur. J. 18 (2012) 4489–4494.
[3] Nathalie Lavoie, Patrick R.L. Malenfant, Fabrice M. Courtel, Yaser Abu-Lebdeh, Isobel J. Davidson, J. Power Sources 213 (2012) 249–254.
[4] Md. Selim Arif Sher Shah, A. Reum Park, Kan Zhang, Jong Hyeok Park, Pil J. Yoo, ACS Appl. Mater. Interfaces 4 (2012) 3893–3901.
[5] Qiwei Tang, Zhongqiang Shan, Li Wang, Xue Qin, Electrochim. Acta 79 (2012) 148–153.
[6] Hua Cheng, Zhou Guang Lu, Jian Qiu Deng, C.Y. Chung, Kaili Zhang, Yang Yang Li, Nano Res. 3 (2010) 895–901.
[7] A. Masao, S. Noda, F. Takasaki, K. Ito, K. Sasaki, Electrochem. Solid State Lett. 12 (2009) B119–B122.
[8] Yuming Chen, Zhouguang Lu, Limin Zhou, Yiu-Wing Mai, Haitao Huang, Energy Environ. Sci. 5 (2012) 7898–7902.
[9] Seung-Min Paek, EunJoo Yoo, Itaru Honma, Nano Lett. 9 (2009) 72–75.
[10] Hongdong Liu, Jiamu Huang, Xinlu Li, Jia Liu, Yuxin Zhang, Kun Du, Appl. Surf. Sci. 258 (2012) 4917–4921.
[11] Zhenyao Wang, Ge Chen, Dingguo Xia, J. Power Sources 184 (2008) 432–436.
[12] Xuyang Wang, Xufeng Zhou, Ke Yao, Jiangang Zhang, Zhaoping Liu, Carbon 49 (2011) 133–139.
[13] Yan Wei, Chao Gao, Fan-Li Meng, Hui-Hua Li, Lun Wang, Jin-Huai Liu, Xing-Jiu Huang, J. Phys. Chem. C 116 (2012) 1034–1041.
[14] Xifei Li, Xiangbo Meng, Jian Liu, Dongsheng Geng, Yong Zhang, Mohammad Norouzi Banis, Yongliang Li, Jinli Yang, Ruying Li, Xueliang Sun, Mei Cai, Mark W. Verbrugge, Adv. Funct. Mater. 22 (2012) 1647–1654.
[15] D.H. Wang, R. Kou, D.W. Choi, Z.G. Ynag, Z.M. Nie, J. Li, L.V. Saraf, D.H. Hu, J. Zhang, G.L. Graff, J. Liu, M.A. Pope, I.A. Aksay, ACS Nano 4 (2010) 1587–1595.
[16] W.S. Hummers, R.E. Offeman, J. Am. Chem. Soc. 80 (1958) 1339.
[17] Yuxi Xu, Kaixuan Sheng, Chun Li, Gaoquan Shi, ACS Nano 4 (2010) 4324–4330.
[18] Enza Fazio, Fortunato Neri, Salvatore Savasta, Phys. Rev. B85 (2012) 195423.
[19] Juan Sun, Cheng Sun, Sudip K. Batabyal, Phong D. Tran, Stevin S. Pramana, Lydia H. Wong, Subodh G. Mhaisalkar, Electrochem. Commun. 15 (2012) 18–21.
[20] Bostjan Genorio, Wei Lu, Ayrat M. Dimiev, Yu Zhu, Abdul-Rahman O. Raji, Barbara Novosel, Lawrence B. Alemany, James M. Tour, ACS Nano 6 (2012) 4231–4249.
[21] Fan-Li Meng, Hui-Hua Li, Ling-Tao Kong, Jin-Yun Liu, Zhen Jin, Wei Li, Yong Jia, Jin-Huai Liu, Xing-Jiu Huang, Anal. Chim. Acta 736 (2012) 100–107.
[22] Zhiyong Wang, Hao Zhang, Nan Li, Zujin Shi, Zhennan Gu, Gaoping Cao, Nano Res. 3 (2010) 748–756.
[23] X.W. Guo, X.P. Fang, Y. Sun, L.Y. Shen, Z.X. Wang, L.Q. Chen, J. Power Sources 226 (2013) 75–81.
[24] Shujiang Ding, Deyan Luan, Freddy Yin Chiang Boey, Jun Song Chen, Xiong Wen (David) Lou, Chem. Commun. 47 (2011) 7155–7157.